Journal of Power Sources 209 (2012) 318–325

Contents lists available at SciVerse ScienceDirect

Journal of Power Sources

journal homepage: www.elsevier.com/locate/jpowsour

Controls oriented reduced order modeling of lithium deposition on overcharge

Roger D. Perkins[a], Alfred V. Randall[a], Xiangchun Zhang[b], Gregory L. Plett[a,*]

[a] Department of Electrical and Computer Engineering, University of Colorado Colorado Springs, Colorado Springs, CO 80918,United States
[b] Sakti3, 1490 Eisenhower Place, Building 4, Ann Arbor, MI 48108-3283, United States

ARTICLE INFO

Article history:
Received 25 October 2011
Received in revised form 1 March 2012
Accepted 2 March 2012
Available online 7 March 2012

Keywords:
Lithium deposition model
Lithium plating model
Lithium ion cell degradation
Incremental reduced order model

ABSTRACT

Battery cell life depends critically on how the cell is used. Therefore, battery chargers and battery management systems must be designed to control cell usage carefully. In order to design optimal battery controls that effect a tradeoff between cell performance (in some sense) and cell life, a model of cell degradation is necessary. This model must be simple and incremental in order to be implemented by an inexpensive microcontroller. This paper takes a first step toward developing such a controls-oriented comprehensive cell degradation model by deriving a reduced-order model of a single mechanism: lithium deposition on overcharge, along with the resulting resistance rise and capacity loss. This reduced-order model approximates a physics-based PDE model from the literature, is simple and accurate, and may be used in optimal strategies for controlling lithium ion batteries.

1. Introduction

Battery packs require monitoring and control to ensure safety, to deliver peak performance, and to maximize life. It is generally necessary to make compromises among these objectives since high charge and discharge rates accelerate aging and can result in unsafe operating conditions. Accordingly, a present goal of our research program is to design battery control methodologies to mathematically optimize a tradeoff between performance and life. To do so, we require quantitative models of the dominant cell degradation mechanisms that can accurately predict a measure of the degradation that would be caused by candidate control actions. These models must be simple enough to be executed quickly on an inexpensive embedded systems processor, so we seek to develop reduced-order approximations to more complex partial-differential equation (PDE) models describing mechanical and chemical cell degradation processes.

Presently, many battery management systems track macroscopic indicators of aging such as capacity fade and power fade but few, if any, track physical indicators of aging such as degree of solid-electrolyte-interphase (SEI) layer growth on anode particles, degree of lithium plating on anode particles, degree of cathode dissolution, and so forth. However, identical combinations of capacity loss and resistance rise might be achieved by traveling different paths—by exciting different physical mechanisms of degradation—yielding potentially different resultant optimal control strategies for operating the battery pack. Therefore, knowing cell resistance and capacity alone is not sufficient to extend cell life to the maximum extent via control.

We believe that by modeling the dominant physical degradation mechanisms that occur in a cell, and then by using those models in an optimized predictive control algorithm, battery life can be extended. For a practical implementation, this requires that the degradation model be *simple* and *incremental*. We consider a model to be simple if it is described by a small number of ordinary difference equations, and incremental (or recursive) if it predicts a future degradation state based on a present degradation state and a proposed cell current. The model will necessarily be a function of cell temperature, state-of-charge (SOC), and possibly other factors as well.

Degradation leading to capacity loss and resistance rise can occur either due to mechanical stress factors or chemical side reactions [1–8]. Various schemes have been introduced to model side reactions, including that of Darling and Newman, who first introduced the concept of modeling parasitic effects in lithium-ion batteries by modeling solvent oxidation side reactions [3]. Here, we focus on overcharge, and on creating a simplified approximation to a model proposed by Arora and colleagues [9]. Overcharge manifests first as a metallic lithium deposit on the surface of the negative electrode solid particles during charge, predominantly near the separator. Subsequently, the lithium can and does further combine with electrolyte material to form other compounds such as Li_2O, LiF, Li_2CO_3, and polyolefins. The nature of the final product is not our major concern in this paper; rather, the issue is that lithium is irreversibly lost. This phenomenon is an unintended side reaction that can lead to severe capacity fade, electrolyte degradation, and a possible safety hazard.

* Corresponding author. Tel.: +1 719 255 3468; fax: +1 719 255 3589.
E-mail addresses: rperkin3@uccs.edu (R.D. Perkins), alfred.randall@colorado.edu (A.V. Randall), xcz@sakti3.com (X. Zhang), gplett@uccs.edu (G.L. Plett).

0378-7753/$ – see front matter © 2012 Elsevier B.V. All rights reserved.
doi:10.1016/j.jpowsour.2012.03.003

The present paper builds on and extends the work in [9] to propose a simple incremental model of overcharge and associated capacity loss and resistance rise. The proposed model may then be used in an optimal control scheme that will reduce side reactions and limit cell degradation. (The control task is the subject of present research, and will be reported in a later paper. The methodology presented in [10] is one possible approach.) While various efforts have been made to create reduced-order models of ideal-cell dynamics (i.e., models that don't consider degradation), including single particle models by Chaturvedi [11] and one-dimensional models by Smith [12], we believe this to be one of the first attempts to create a reduced-order model to describe a side reaction. This reduced-order model of overcharge is a first step toward creating a complete coupled reduced-order model of all dominant cell degradation mechanisms, which then could be used in an optimal control scheme.

This paper will proceed by reviewing the model of overcharge proposed in [9]. A reduced-order one-dimensional approximate model is then derived. Results of pulsed-current simulations of the full-order model and the reduced-order model are presented and compared, results are discussed, and conclusions are made.

2. Physics-based model of overcharge

Changes at the electrode/electrolyte interface due to side reactions between the anode and electrolyte are considered to be one of the primary causes of anode aging [8]. One particularly severe degradation mechanism is that of overcharge, where metallic lithium plates on the electrode surface. A physics-based coupled PDE model of ideal-cell and overcharge dynamics has been reported in [9]. Our goal is to create a high-fidelity reduced-order model of this PDE degradation model; therefore, we adopt the same assumptions as they, which were:

1. The main side reaction is expressed as $Li^+ + e^- \rightarrow Li(s)$, which occurs at $U_s = 0$ V versus Li/Li^+ during an overcharge event. This lithium metal is expected to form first near the electrode-separator boundary where the surface overpotential is greatest.
2. Lithium metal deposited on the negative electrode reacts quickly with solvent or salt molecules in the vicinity, yielding Li_2CO_3, LiF, or other insoluble products. A thin film of these products protects the solid lithium from reacting with the electrolyte. Solid lithium can still dissolve during discharge, but once lithium is consumed in a insoluble product, it is permanently lost.
3. The insoluble products formed are a mixture of different species, resulting in averaged mass and density constants used in a later equation describing the formation and growth of a resistive film.
4. Only the overcharge reaction is considered (e.g., SEI film growth and other degradation mechanisms are not modeled).

The overcharge model of [9] is tightly coupled with a "pseudo two-dimensional" Doyle–Fuller–Newman porous-electrode style model of ideal-cell dynamics [4], which assumes that the solid and electrolyte phases are considered continuous and gives no consideration to the underlying microstructure of the electrode. While porous-electrode theory is well known, there are variants in its implementation, so we present the full set of model equations here, in summary form. We list the model in terms of the negative electrode only; all equations have exact analogs for the positive electrode as well, with the exception of the lithium plating equations, as plating happens only on the negative electrode. Symbols are defined in a table at the end of this paper; only the most relevant are identified here.

The conservation of lithium in a single particle is modeled by Fick's law of diffusion

$$\frac{\partial c_s(r,x,t)}{\partial t} = \frac{D_s}{r^2}\frac{\partial}{\partial r}\left(r^2\frac{\partial c_s(r,x,t)}{\partial r}\right),$$

with boundary conditions

$$\left.\frac{\partial c_s(r,x,t)}{\partial r}\right|_{r=0} = 0 \quad \text{and} \quad D_s\left.\frac{\partial c_s(r,x,t)}{\partial r}\right|_{r=R} = \frac{-j_n(x,t)}{a_s F},$$

where $j_n(x,t)$ is the intercalation current density. Conservation of lithium in the electrolyte phase gives the following equation,

$$\frac{\partial c_e(x,t)}{\partial t} = \frac{\partial}{\partial x}\left(\frac{D_e^{\text{eff}}}{\varepsilon_e}\frac{\partial c_e(x,t)}{\partial x}\right) + \frac{(1-t_0^+)}{F\varepsilon_e}\frac{\partial i_e(x,t)}{\partial x}, \tag{1}$$

where $D_e^{\text{eff}} = D_e\varepsilon_e^{\text{brug}}$ and having the following zero flux boundary conditions at the current collectors,

$$\left.\frac{\partial c_e(x,t)}{\partial x}\right|_{x=0} = \left.\frac{\partial c_e(x,t)}{\partial x}\right|_{x=L} = 0. \tag{2}$$

In Eq. (1), the current density in the electrolyte has the form,

$$\frac{\partial i_e(x,t)}{\partial x} = j_{\text{total}}(x,t), \tag{3}$$

where $j_{\text{total}}(x,t) = j_n(x,t) + j_s(x,t)$ and $j_s(x,t)$ is the side-reaction current density. Eq. (3) has the boundary conditions

$$i_e(0,t) = 0 \quad \text{and} \quad i_e(L_n,t) = \frac{I(t)}{A}, \tag{4}$$

where $I(t)$ is the cell current and A is the current-collector area. Current density in the solid has the form

$$i_s(x,t) = \frac{I(t)}{A} - i_e(x,t). \tag{5}$$

Charge conservation in the solid phase in the electrodes is described by Ohm's law,

$$-\sigma^{\text{eff}}\frac{\partial}{\partial x}\phi_s(x,t) = i_s(x,t), \tag{6}$$

where $\sigma^{\text{eff}} = \sigma\varepsilon_s^{\text{brug}}$, $\phi_s(0,t) = 0$ by convention, and having boundary conditions at the current collector and separator boundaries,

$$-\sigma^{\text{eff}}\left.\frac{\partial\phi_s(x,t)}{\partial x}\right|_{x=0} = \frac{I(t)}{A} \quad \text{and} \quad \left.\frac{\partial\phi_s(x,t)}{\partial x}\right|_{x=L_n} = 0. \tag{7}$$

Conservation of charge in the electrolyte gives the equation

$$\frac{\partial\phi_e(x,t)}{\partial x} = \frac{-i_e(x,t)}{\kappa^{\text{eff}}} - \frac{\kappa_D^{\text{eff}}}{\kappa^{\text{eff}}}\frac{\partial \ln c_e(x,t)}{\partial x}, \tag{8}$$

where $\kappa^{\text{eff}} = \kappa\varepsilon_e^{\text{brug}}$, $\kappa_D^{\text{eff}} = (2R_gT\kappa^{\text{eff}}/F)(t_+^0 - 1)$, and having boundary conditions

$$\left.\frac{\partial\phi_e(x,t)}{\partial x}\right|_{x=0} = \left.\frac{\partial\phi_e(x,t)}{\partial x}\right|_{x=L} = 0.$$

The PDEs are coupled via the intercalation current density, expressed as the Butler–Volmer equation,

$$j_n(x,t) = a_n i_{0,n}\left[\exp\left(\frac{\alpha_{a,n}F}{R_gT}\eta_n(x,t)\right) - \exp\left(-\frac{\alpha_{c,n}F}{R_gT}\eta_n(x,t)\right)\right] \tag{9}$$

which is driven by the overpotential

$$\eta_n(x,t) = \phi_s(x,t) - \phi_e(x,t) - U_n - \frac{j_n(x,t)}{a_n}R_{\text{film}},$$

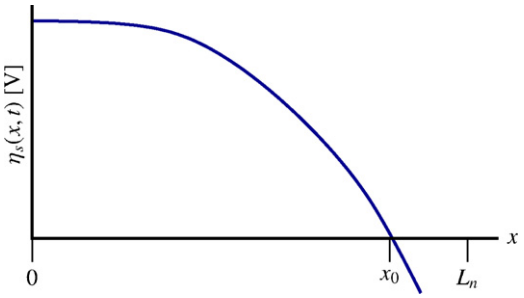

Fig. 1. Typical profile of side-reaction overpotential during overcharge.

where $i_{0,n}$ is the exchange current density,

$$i_{0,n} = k_n(c_{s,n}^{\max} - c_{s,n})^{\alpha_{a,n}}(c_{s,n})^{\alpha_{c,n}}(c_e)^{\alpha_{a,n}},$$

and U_n is the equilibrium potential which is evaluated as a function of the solid phase concentration at the surface of the particle.

With this "ideal-cell" (no degradation) model in place, it is straightforward to add the terms that account for lithium plating. The side-reaction current density j_s (i.e., the rate of irreversible lithium loss due to lithium plating) can be expressed as

$$j_s(x,t) = \min\left(0, a_n i_{o,s}\left[\exp\left(\frac{\alpha_{a,s}F}{R_gT}\eta_s(x,t)\right) - \exp\left(-\frac{\alpha_{c,s}F}{R_gT}\eta_s(x,t)\right)\right]\right), \quad (10)$$

where $\alpha_{a,s} \neq \alpha_{c,s}$ in general,

$$\eta_s(x,t) = \phi_s(x,t) - \phi_e(x,t) - U_s - \frac{j_s(x,t)}{a_n}R_{\text{film}},$$

and where the side-reaction exchange current density $i_{0,s} = k_{n,s}(c_e)^{\alpha_{a,s}}$. The side reaction is semi-irreversible in the sense that it includes an anodic rate term, but does not allow an overall positive side-reaction current density. The side reaction occurs only at spatial locations in the anode where $\eta_s(x,t) < 0$. This is enforced in Eq. (10) by the "min" function, which sets $j_s(x,t) = 0$ for values of x where $\eta_s(x,t) \geq 0$, but to the value computed by the Butler–Volmer equation when $\eta_s(x,t) < 0$. A typical scenario is plotted in Fig. 1, where $\eta_s(x,t)$ is sketched across the electrode width. In this example, plating will occur in the interval from $x = x_0$ to $x = L_n$. Note that this illustration shows that the cell can be quite far away from 100% state-of-charge and still have plating occur near the separator if a large enough charge current pulse is applied to the cell's terminals. The state-of-charge is only one variable of importance—ultimately, the local overpotential determines whether plating occurs.

Once the local side reaction current has been calculated, the change in the film thickness δ_{film} during charging is modeled as

$$\frac{\partial \delta_{\text{film}}(x,t)}{\partial t} = -\frac{M}{a_n \rho F} j_s(x,t), \quad (11)$$

where M and ρ are the average molecular weight and density of lithium and products. The resistance $R_{\text{products}}(x,t)$ of the film formed by lithium and other products (Li_2CO_3 is used as an example here) is given by

$$R_{\text{products}}(x,t) = z_{\text{Li}}\left(\frac{\delta_{\text{film}}(x,t)}{\kappa_{\text{Li}}}\right) + z_{\text{Li}_2\text{CO}_3}\left(\frac{\delta_{\text{film}}(x,t)}{\kappa_{\text{Li}_2\text{CO}_3}}\right)$$

where z_{Li} and $z_{\text{Li}_2\text{CO}_3}$ are the volume fractions of lithium and Li_2CO_3 present in the film. The film resistance is then given by

$$R_{\text{film}}(x,t) = R_{\text{SEI}}^0(x,t) + R_{\text{products}}(x,t) \quad (12)$$

where R_{SEI}^0 is the initial film resistance that is produced during the formation period of the battery.

In addition to the resistance change, there is a capacity loss caused by the side reaction current during charge, leading to capacity changing via the relationship

$$\frac{\partial Q(t)}{\partial t} = A\int_0^{L_n} j_s(x,t)\,dx. \quad (13)$$

3. Derivation of reduced order model and plating prediction equations

To effect an optimal control strategy, the processors in battery chargers and battery management systems must be able to calculate the rate of lithium loss due to overcharge very quickly and accurately. Solving the coupled PDE equations described above is too complicated for such a process. The degradation model needs to be much faster and simpler. In this section, we present a simpler incremental model for calculating $j_s(x,t)$, $R_{\text{film}}(t)$, and $Q(t)$, which yields an algebraic rather than differential solution.

To create the reduced-order model, several additional assumptions are made:

1. The cell is always in a quasi-equilibrium state, allowing the exchange current density $i_{0,n}$ to be calculated from the cell SOC alone, neglecting local variations in electrolyte and solid surface concentration. The estimated value of $j_s(x,t)$ then corresponds to a suddenly applied current pulse of magnitude $I(t)$, which is constant over some time interval Δt.
2. The total current density is uniform over the anode: $j_{\text{total}}(x,t) = \bar{j}_{\text{total}}(t)$. This assumption decides the solution profile of other variables. The solution profile inside of batteries will be more complicated, and the results section investigates the accuracy lost by making this assumption.
3. We model the short-term time rate of change of concentration of lithium in the electrolyte as proportional to the applied current spread out over the electrode: $\partial c_e(x,t)/\partial t \approx \beta I(t)/(FAL_n)$.
4. We assume that the absolute variation in lithium concentration in the electrolyte is negligible in comparison to its gradient. This allows us to write $\partial \ln c_e(x,t)/\partial x = (1/c_e(x,t))(\partial c_e(x,t)/\partial x) \approx (1/\bar{c}_e)(\partial c_e(x,t)/\partial x)$, where $\bar{c}_e$ is the volume-average concentration of lithium in the electrolyte.
5. The anodic and cathodic charge-transfer coefficients of the intercalation kinetics are equal ($\alpha_{n,a} = \alpha_{n,c} = 0.5$).

With these models and assumptions in mind, we take the following steps to derive the rate of lithium loss due to overcharge:

1. We derive the ionic current $i_e(x,t)$ by integrating Eq. (3).
2. We show that $\phi_s(x,t) \approx 0$ at all points in the negative electrode.
3. We substitute $i_e(x,t)$ into Eq. (1) to determine the electrolyte concentration gradient $\partial c_e(x,t)/\partial x$.
4. We substitute $i_e(x,t)$ and $\partial c_e(x,t)/\partial t$ into Eq. (8) to determine the electrolyte potential $\phi_e(x,t)$.
5. Finally, we determine the rate of lithium loss due to overcharge from $\phi_s(x,t) - \phi_e(x,t)$.

3.1. Determining the ionic current

To determine the ionic current, we integrate Eq. (3) across a portion of the negative electrode. We employ Liebnitz' integration rule to correctly deal with the variable integration limits, resulting in:

$$\begin{aligned}\int_0^x \frac{\partial i_e(\chi,t)}{\partial \chi}\,\mathrm{d}\chi &= \int_0^x j_{\text{total}}(\chi,t)\,\mathrm{d}\chi\\ i_e(x,t) - \underbrace{i_e(0,t)}_{0,\ \text{by Eq.(4)}} &= \bar{j}_{\text{total}}(t)x\\ i_e(x,t) &= \bar{j}_{\text{total}}(t)x, \quad 0 \le x \le L_n.\end{aligned}$$

Since $i_e(L_n, t) = I(t)/A$ by Eq. (4), we have that $\bar{j}_{\text{total}}(t) = I(t)/(AL_n)$. With this substitution, we arrive at

$$i_e(x,t) = \frac{I(t)}{AL_n}x. \tag{14}$$

Note that the sign of $I(t)$ is negative during charge, and positive during discharge.

3.2. Showing that $\phi_s(x,t) \approx 0$

We can now solve for the solid potential. Integrating Eq. (6) and employing Eqs. (5) and (14) gives

$$\begin{aligned}-\sigma^{\text{eff}}\int_0^x \frac{\partial}{\partial \chi}\phi_s(\chi,t)\,\mathrm{d}\chi &= \int_0^x i_s(\chi,t)\,\mathrm{d}\chi\\ \phi_s(x,t) - \underbrace{\phi_s(0,t)}_{0} &= -\frac{1}{\sigma^{\text{eff}}}\int_0^x \frac{I(t)}{A}\left[1-\frac{\chi}{L_n}\right]\mathrm{d}\chi\\ \phi_s(x,t) &= -\frac{I(t)}{\sigma^{\text{eff}}A}\left[x - \frac{x^2}{2L_n}\right], \quad 0 \le x \le L_n.\end{aligned} \tag{15}$$

The value of $\phi_s(x, t)$ is later used in determining whether plating occurs by comparison with $\phi_e(x, t)$. Due to the high conductivity of the solid versus the electrolyte, we find that $\phi_s(x)$ is in the order of microvolts, while $\phi_e(x, t)$ is in the order of millivolts. Therefore, we proceed by assuming $\phi_s(x, t) \approx 0$. However, Eq. (15) could be used instead.

3.3. Determining the electrolyte concentration gradient

It is necessary to correlate the applied current to the change of concentration in the electrolyte. Integration of the concentration dynamics Eq. (1) across a portion of the negative electrode, applying Assumption 3, gives

$$\begin{aligned}\int_0^x \frac{\partial c_e(\chi,t)}{\partial t}\,\mathrm{d}\chi = \frac{D_e^{\text{eff}}}{\varepsilon_e}\int_0^x \frac{\partial c_e^2(\chi,t)}{\partial \chi^2}\,\mathrm{d}\chi + \frac{(1-t_0^+)}{F\varepsilon_e}\int_0^x \frac{\partial i_e(\chi,t)}{\partial \chi}\,\mathrm{d}\chi\\ \frac{\beta I(t)}{FAL_n}x = \frac{D_e^{\text{eff}}}{\varepsilon_e}\left[\frac{\partial c_e(x,t)}{\partial x} - \underbrace{\frac{\partial c_e(0,t)}{\partial x}}_{0\ \text{by Eq.(2)}}\right] + \frac{(1-t_0^+)}{F\varepsilon_e}\frac{I(t)}{AL_n}x\end{aligned} \tag{16}$$

$$\frac{\partial c_e(x,t)}{\partial x} = \frac{\beta\varepsilon_e - (1-t_0^+)}{D_e^{\text{eff}}F}\frac{I(t)}{AL_n}x, \quad 0 \le x \le L_n. \tag{17}$$

Note that the gradient of concentration is linear in x, thus implying the concentration itself is parabolic in x across the electrode. We find this to be a very good approximation to the continuum model of a cell.

3.4. Determining the electrolyte potential

With concentration of the electrolyte derived, development of the electrolyte potential can proceed. Substitute Eqs. (17) and (14) into Eq. (8) and employ Assumption 4 to derive the potential of the electrolyte across the electrode:

$$\begin{aligned}\frac{\partial \phi_e(x,t)}{\partial x} &= \frac{-i_e(x,t)}{\kappa^{\text{eff}}} - \frac{\kappa_D^{\text{eff}}}{\kappa^{\text{eff}}}\frac{\partial \ln c_e(x,t)}{\partial x} = \frac{-I(t)}{\kappa^{\text{eff}}AL_n}x - \frac{\kappa_D^{\text{eff}}}{\kappa^{\text{eff}}\bar{c}_e}\frac{\partial c_e(x,t)}{\partial x}\\ &= -\left[\frac{\kappa_D^{\text{eff}}}{\bar{c}_e}\frac{\beta\varepsilon_e - (1-t_0^+)}{D_e^{\text{eff}}F} + 1\right]\frac{I(t)}{\kappa^{\text{eff}}AL_n}x, \quad 0 \le x \le L_n.\end{aligned} \tag{18}$$

The gradient of the electrolyte potential is linear in x, meaning that the electrolyte potential itself is parabolic in x. This is again a very good approximation to the full order model of a cell.

We will integrate once again to determine $\phi_e(x, t)$. However, we first clean up notation by defining

$$E(t) = -\left[\frac{\kappa_D^{\text{eff}}}{\bar{c}_e}\frac{\beta\varepsilon_e - (1-t_0^+)}{D_e^{\text{eff}}F} + 1\right]\frac{I(t)}{\kappa^{\text{eff}}AL_n}. \tag{19}$$

Then, $\partial\phi_e(x, t)/\partial x = E(t)x$. We integrate this expression to find $\phi_e(x, t)$

$$\begin{aligned}\int_0^x \frac{\partial \phi_e(\chi,t)}{\partial \chi}\,\mathrm{d}\chi &= \int_0^x E(t)\chi\,\mathrm{d}\chi\\ \phi_e(x,t) - \phi_e(0,t) &= \frac{E(t)}{2}x^2\\ \phi_e(x,t) &= \frac{E(t)}{2}x^2 + \phi_e(0,t), \quad 0 \le x \le L_n.\end{aligned} \tag{20}$$

To complete the calculation of $\phi_e(x, t)$, we must determine $\phi_e(0, t)$. To do so, we select the value of $\phi_e(0, t)$ that will result in the average $\phi_e(x, t)$ across the length of the anode $\overline{\phi_e}(t)$ being equal to the expected average. The expected average is found by inverting the Butler–Volmer Eq. (9), and by finding the value of $\bar{\eta}$ that results in $\bar{j}_n$. This is easily done if $\alpha_{a,n} = \alpha_{c,n} = 0.5$ (cf. Assumption 5), when

$$\bar{\eta}(t) = \frac{2R_gT}{F}\operatorname{asinh}\left(\frac{\bar{j}_n(t)}{2a_ni_{0,n}}\right). \tag{21}$$

Then, $\overline{\phi_e}(t) = -(\bar{\eta}(t) + U_n + \bar{j}_n(t)R_{\text{film}}/a_n)$.

To use this result to determine $\phi_e(0, t)$, we must calculate the corresponding value of $\overline{\phi_e}(t)$ from Eq. (20).

$$\begin{aligned}\overline{\phi_e}(t) &= \frac{1}{L_n}\int_0^{L_n}\phi_e(x,t)\,\mathrm{d}x = \frac{1}{L_n}\left[\frac{E(t)}{6}x^3 + \phi_e(0,t)x\right]\Big|_0^{L_n} = \frac{E(t)}{6}L_n^2 + \phi_e(0,t)\\ \phi_e(0,t) &= \overline{\phi_e}(t) - \frac{E(t)}{6}L_n^2 = -\left(\frac{2R_gT}{F}\operatorname{asinh}\left(\frac{\bar{j}_n(t)}{2a_ni_{0,n}}\right) + U_n + \frac{\bar{j}_n(t)R_{\text{film}}}{a_n}\right)\\ &\quad - \frac{E(t)}{6}L_n^2.\end{aligned} \tag{22}$$

Finally, this gives us the equation

$$\begin{aligned}\phi_e(x,t) = \frac{E(t)}{2}x^2 - \left(\frac{2R_gT}{F}\operatorname{asinh}\left(\frac{\bar{j}_n(t)}{2a_ni_{0,n}}\right) + U_n + \frac{\bar{j}_n(t)R_{\text{film}}}{a_n}\right)\\ - \frac{E(t)}{6}L_n^2.\end{aligned}$$

Once again, to ease notation we define

$$P(t) = \frac{E(t)}{6}L_n^2 + \left(\frac{2R_gT}{F}\operatorname{asinh}\left(\frac{\bar{j}_n(t)}{2a_ni_{0,n}}\right) + U_n + \frac{\bar{j}_n(t)R_{\text{film}}}{a_n}\right), \tag{23}$$

which allows us to write

$$\phi_e(x,t) = \frac{E(t)}{2}x^2 - P(t). \tag{24}$$

3.5. Plating equations

Lithium plating occurs only during charge, and at any point along the anode where $\eta_s(x, t) < 0$ (by Eq. (10)). As we are

assuming that $\phi_s(x, t) \approx 0$ and $U_s = 0$, plating occurs where $\phi_e(x, t) + (j_s(x, t)R_{\text{film}}/a_n) > 0$. The parabolic shape of Eq. (24) means that if $\phi_e(0, t) > -j_s(x, t)R_{\text{film}}/a_n$ during charge, there is plating across the entire width of the anode. If $\phi_e(L_n, t) < -j_s(x, t)R_{\text{film}}/a_n$, then there is no plating at any location across the width of the anode. Otherwise, there is plating that occurs across a region from x_0 to L_n, where x_0 is a value yet to be determined.

To find the location where plating begins, we solve for $\phi_e(x_0, t) = -\bar{j}_s(t)R_{\text{film}}/a_n$.

$$\begin{aligned}\frac{E(t)}{2}x_0^2 &= P(t) - \frac{\bar{j}_s(t)R_{\text{film}}}{a_n}\\ x_0 &= \sqrt{2\frac{P(t) - \bar{j}_s(t)R_{\text{film}}/a_n}{E(t)}}.\end{aligned}$$

We "spread out" the plating region over the electrode width to get an equivalent overpotential,

$$\begin{aligned}\bar{\eta}_{s,oc}(t) &= \frac{1}{L_n}\int_{x_0}^{L_n} -\phi_e(x, t) - \frac{\bar{j}_s(t)R_{\text{film}}}{a_n}\ \mathrm{d}x\\ &= -\frac{1}{L_n}\int_{x_0}^{L_n} \frac{E(t)}{2}x^2 - P(t) + \frac{\bar{j}_s(t)R_{\text{film}}}{a_n}\ \mathrm{d}x\\ &= -\frac{1}{L_n}\left[\frac{E(t)}{6}x^3 - P(t)x + \frac{\bar{j}_s(t)R_{\text{film}}}{a_n}x\right|_{x_0}^{L_n}\\ &= -\frac{1}{L_n}\left[\frac{E(t)}{6}(L_n^3 - x_0^3) - P(t)(L_n - x_0) + \frac{\bar{j}_s(t)R_{\text{film}}}{a_n}(L_n - x_0)\right].\end{aligned} \tag{25}$$

The side-reaction deposition current from overcharge is also described by the Butler–Volmer equation, except in this case the anodic and cathodic transfer coefficient are typically not equal and the reaction is favored to be cathodic:

$$\bar{j}_s(t) = a_n i_{0,s}\left[\exp\left(\frac{\alpha_{a,s}F}{R_gT}\bar{\eta}_{s,oc}(t)\right) - \exp\left(-\frac{\alpha_{c,s}F}{R_gT}\bar{\eta}_{s,oc}(t)\right)\right]. \tag{26}$$

3.6. Summary of method

Here we summarize the complete method for determining the rate of lithium loss. The method is iterative, requiring that $\bar{j}_n(t) + \bar{j}_s(t) = \bar{j}_{\text{total}}(t)$. We initialize the iteration with $\bar{j}_s(t) = 0$.

1. Compute $i_{0,n}$ based on the present cell state of charge and set $\bar{j}_s(t) = 0$.
2. Compute

$$E(t) = -\left[\frac{\kappa_D^{\text{eff}}}{\bar{c}_e}\frac{\beta\varepsilon_e - (1 - t_0^+)}{D_e^{\text{eff}}F} + 1\right]\frac{I(t)}{\kappa^{\text{eff}}AL_n}.$$

3. Set $\bar{j}_n(t) = (I(t)/(AL_n)) - \bar{j}_s(t)$.
4. Compute

$$P(t) = \frac{E(t)}{6}L_n^2 + \frac{2R_gT}{F}\operatorname{asinh}\left(\frac{\bar{j}_n(t)}{2a_n i_{0,n}}\right) + U_n + \frac{\bar{j}_n(t)R_{\text{film}}}{a_n}.$$

5. Compute

$$x_0 = \begin{cases} 0, & P(t) < \dfrac{\bar{j}_s(t)R_{\text{film}}}{a_n};\\ L_n, & E(t)L_n^2 < 2P(t) - 2\dfrac{\bar{j}_s(t)R_{\text{film}}}{a_n};\\ \sqrt{2\dfrac{P(t) - \bar{j}_s(t)R_{\text{film}}/a_n}{E(t)}}, & \text{otherwise.}\end{cases}$$

6. Compute

$$\bar{\eta}_{s,oc}(t) = -\frac{1}{L_n}\left[\frac{E(t)}{6}(L_n^3 - x_0^3) - P(t)(L_n - x_0) + \frac{\bar{j}_s(t)R_{\text{film}}}{a_n}(L_n - x_0)\right].$$

7. Compute

$$\bar{j}_s(t) = \begin{cases} a_n i_{0,s}\left[\exp\left(\dfrac{\alpha_{a,s}F}{R_gT}\bar{\eta}_{s,oc}(t)\right) - \exp\left(-\dfrac{\alpha_{c,s}F}{R_gT}\bar{\eta}_{s,oc}(t)\right)\right], & x_0 < L_n\\ 0, & x_0 = L_n.\end{cases}$$

8. Iterate steps 3–7 until $|\bar{j}_n(t) + \bar{j}_s(t) - (I(t)/(AL_n))| < \epsilon$, where ϵ is a convergence factor.

The iteration in step 8 is generally done using a nonlinear solver. In our results, we used a quasi-Newton approach.

Once we have solved for $\bar{j}_s(t)$ it can then be incorporated into incremental equations for film resistance and capacity loss. It is assumed that $\bar{j}_s(t)$ is constant over some small time interval Δt, and is denoted as $\bar{j}_s[N]$ for the Nth interval. Since, according to Eq. (11), the change in film thickness is proportional to $\bar{j}_s$, we can arrive at an incremental equation for film thickness as

$$\bar{\delta}_{\text{film}}[N] = \bar{\delta}_{\text{film}}[N - 1] - \frac{M\Delta t}{a_n\rho F}\bar{j}_s[N - 1],$$

where Δt is the equation update period, and noting that the sign of $\bar{j}_s$ is negative. This result can be used to calculate the film resistance as

$$\bar{R}_{\text{film}}[N] = \bar{R}_{\text{film}}[N - 1] - \frac{MR_{\text{equiv}}\Delta t}{a_n\rho F}\bar{j}_s[N - 1],$$

where $R_{\text{equiv}} = z_{\text{Li}}/\kappa_{\text{Li}} + z_{\text{Li}_2\text{CO}_3}/\kappa_{\text{Li}_2\text{CO}_3}$. Similarly, we can discretize the capacity equation (13) to find that

$$Q[N] = Q[N - 1] + (AL_n\Delta t)\bar{j}_s[N - 1].$$

4. Simulation and results

The validity of this reduced-order model depends first on the accuracy of the underlying partial differential equation model, which we assume here to be exact. It then depends on how closely the reduced-order approximation of $\bar{j}_s$ matches the exact calculation of $\bar{j}_s$. In this section, results from both the full and reduced-order models for $\bar{j}_s$ are compared.

To compare the PDE and reduced-order models, we conducted a series of simulations. In each simulation, the cell was initially at rest. A sudden pulse of current was then applied, and the resulting $\bar{j}_s$ from the PDE model, averaged over a 1-s interval subsequent to the pulse, was compared to the computed $\bar{j}_s$ from the ROM. To simulate the PDE model, we used COMSOL Multiphysics 3.5a [13] coupled with a MATLAB [14] script to cycle through the series of simulations and analyze results. Specifically, each simulation comprised a 1.2 s time interval, where the cell current i_{app} was modeled as a step function, which was applied at $t = 0.2$ s. We found that the initial rest interval facilitated convergence of the solution by allowing the PDE solver to adjust its initial conditions before applying the

Table 1
Electrode parameters for simulation.

Symbol	Units	Anode	Separator	Cathode
L	μm	85	76.2	179.3
R	μm	12.5	–	8.5
A	m^2	1	1	1
σ	$S\,m^{-1}$	100	–	3.8
ε_s	–	0.59	–	0.534
ε_e	–	0.36	1	0.416
κ_e	$S\,m^{-1}$	0.2875	0.2875	0.2875
brug	–	1.5	–	1.5
c_s^{max}	$mol\,m^{-3}$	30 540	–	22 860
c_e^0	$mol\,m^{-3}$	1000	1000	1000
$\theta_{i,min}$	–	0.10	–	0.95
$\theta_{i,max}$	–	0.90	–	0.175
D_s	$m^2\ s^{-1}$	2.0×10^{-14}	–	1.0×10^{-13}
D_e	$m^2\ s^{-1}$	7.5×10^{-11}	7.5×10^{-11}	7.5×10^{-11}
t_+^0	–	0.363	0.363	0.363
k	$A\,m^{5/2}\ mol^{-3/2}$	2×10^{-6}	–	2×10^{-6}
α_a	–	0.5	–	0.5
α_c	–	0.5	–	0.5
$\alpha_{a,s}$	–	0.3	–	–
$\alpha_{c,s}$	–	0.7	–	–
$U_{ref,s}$	V	0.0	–	–
R_{SEI}	$\Omega\,m^2$	0.002	–	–
$i_{0,s}$	$A\,m^{-2}$	10	–	–

step current. (Even so, convergence of the PDE simulations proved troublesome, and required user vigilance to ensure reliable results.) The solver absolute tolerance was set to 10^{-1} and the relative tolerance to 10^{-3}. The default direct UMFPACK solver was used, with 106 mesh points in the 1D battery model and 7056 elements in the 2D electrode model. The solver timestep was set to 20 ms. The ROM results were computed by a MATLAB script using the method summarized in Section 3.6.

The cell parameters that we used in the simulations match those used in [9] and are listed in Table 1. The applied current was varied between 0 C and 3 C in increments of C/33; the initial cell SOC was varied between 0% and 100% in steps of 1%, and temperature was held constant at 25 °C. We found that the adjustable tuning factor $\beta = 1.7$ worked well (this implies the change in electrolyte concentration near the separator changes nearly twice as quickly as it does near the current collector). A total of 10 100 simulations were run. As one point of comparison, the set of full-order PDE simulations took approximately 12 h to complete, utilizing an average of three cores, on an Intel i7 processor, while the set ROM simulations took approximately 21 s to complete, utilizing an average of one core on the same machine. The speedup, on a per-simulation per-core basis, is more than 5000 : 1. This is the primary advantage of the ROM over the PDE model.

Lithium plating occurs when the side-reaction overpotential is negative ($\eta_s < 0$). Fig. 2(a) illustrates the side-reaction overpotential across the anode for this cell model, where $x = 0$ is adjacent to the current-collector and $x = 85$ μm is adjacent to the separator, immediately following the onset of a charge current pulse. From the PDE result, we expect lithium deposit to occur between about $x = 42$ μm and $x = 85$ μm. From the ROM, we expect lithium deposit to occur between $x_0 = 49$ μm and $x = 85$ μm. Fig. 2(b) shows the resulting rate of lithium deposition for the PDE and ROM solutions. The time-average deposition rate of the ROM is somewhat higher than the time-average deposition rate of the PDE over the 1 s interval.

Fig. 3 illustrates the predicted overcharge rates over all scenarios for the PDE and the ROM solutions. As expected, deposition is worse at high SOC and high charge rates. The PDE and ROM solutions generally agree very well, with greatest mismatch at high charge rates.

Fig. 4 shows a different view of Fig. 3. Cross sections through both the PDE and ROM solution spaces are plotted and compared.

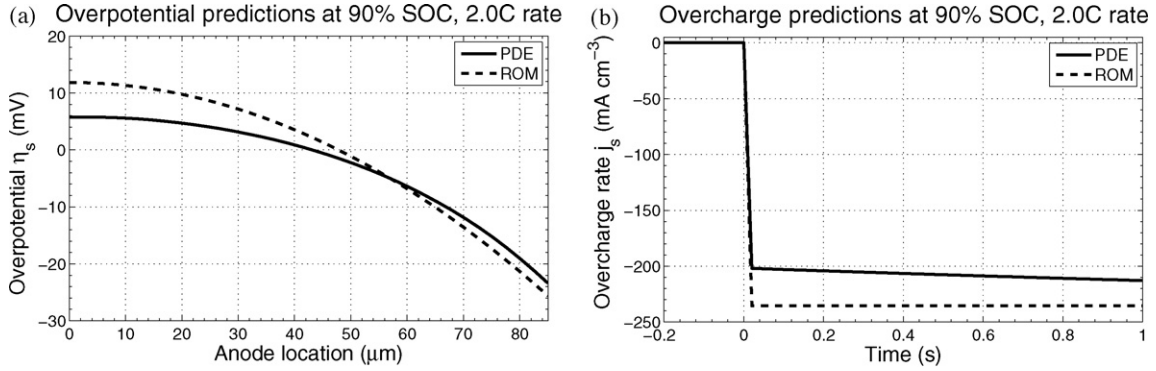

Fig. 2. Comparing PDE and ROM overpotential and deposition-rate predictions.

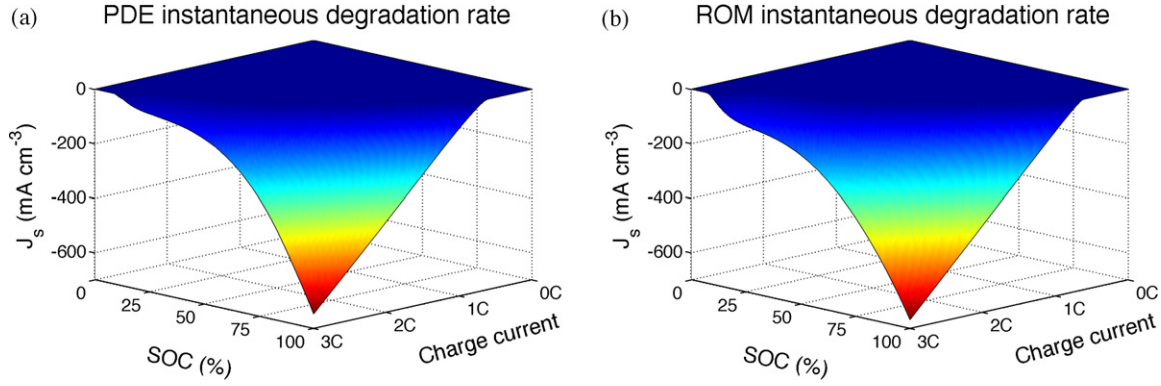

Fig. 3. Comparing the PDE and ROM over multiple scenarios.

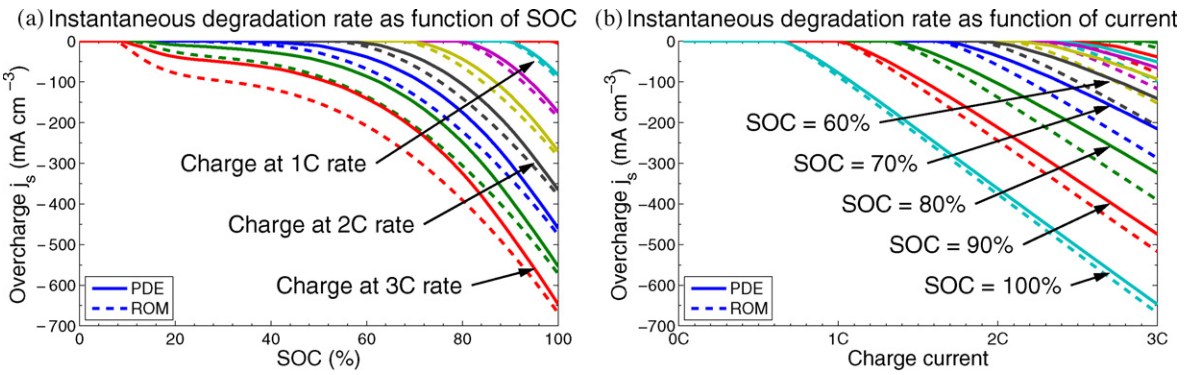

Fig. 4. Cross sections through the plots in Fig. 3 to more clearly illustrate effects of SOC and rate.

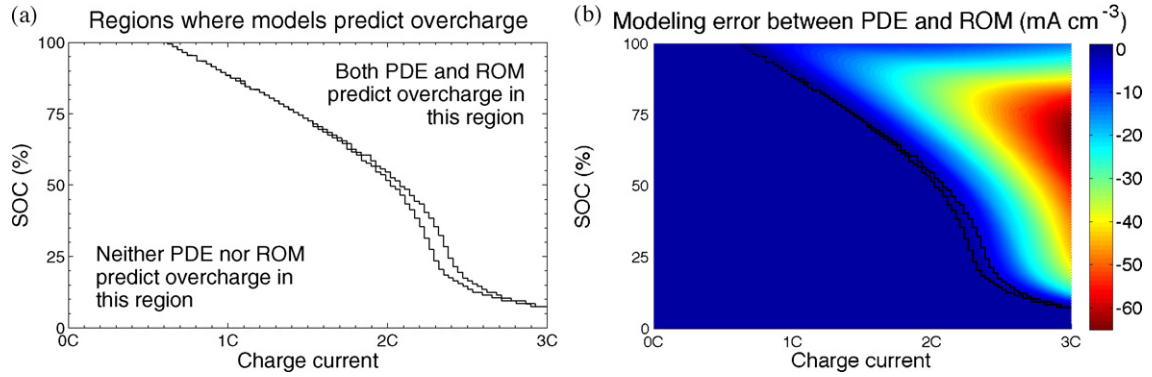

Fig. 5. Comparing the PDE and ROM solutions.

Frame (a) shows how the two methods compare where each pair of lines represents a specific charge rate. As noted before, but perhaps more clearly seen here, the difference between the PDE and ROM solutions are greatest at high charge rates. Frame (b) shows how the two methods compare where each pair of lines represents a specific initial SOC. The difference is greatest at moderate SOC levels.

Finally, Fig. 5 illustrates the error between the PDE and ROM solutions in two ways. Frame (a) shows the regions where the two methods agree on whether lithium deposition will occur, and the region where they disagree. The region of disagreement is the very narrow sliver at around 2.4 C and 25% SOC, where the ROM predicts overcharge but the PDE does not. Otherwise, the boundaries are identical. Frame (b) shows the error between the solutions, calculated as $\bar{j}_{s,\mathrm{ROM}} - \bar{j}_{s,\mathrm{PDE}}$. The maximum error is approximately 65 mA cm^{-2}. When compared to Fig. 3, we see that the relative error is on the order of 10%.

For the purpose of control system design, the results of Fig. 5(a) are the most important. Since lithium deposition is such a severe degradation mechanism, a charging control scheme should avoid ever commanding a control action that would cause any lithium deposition to occur. A time-optimal charger, based only on the PDE model of lithium deposition, would select charge pulse current to follow the upper contour in Fig. 5(a). This allows the maximum charge rate at any point in time, while causing no lithium plating. In comparison, a time-optimal charger, based only on the ROM model of lithium deposition, would select charge pulse current to follow the lower contour in the figure. This will result in somewhat slower charging. But, because the ROM over-predicts the amount of lithium deposition, it will also result in a charging scheme that is conservative, which is a beneficial feature.

We conducted additional simulations to investigate the effect of pulse length Δt in Assumption 1 of Section 3. That is, how long can the charge pulse be before the full-order PDE model and the reduced order model results are significantly different? We found that pulse lengths less than 10 s are generally well matched, but pulse lengths much greater than 10 s can give significant PDE versus ROM mismatch. For long pulse durations, the quasi-static nature of Assumption 1 is violated, and an a significant offset is noted in actual time-varying ϕ_e versus the at-rest ϕ_e, moving the crossover point of $\eta_s(x, t)$. This causes the ROM to under predict the value of lithium plating computed by the PDE. For this reason, we propose that the ROM is of most value for computing current limits in dynamic applications such as hybrid-electric vehicles, where a bias in ϕ_e cannot develop due to the random nature of power demand, but is of less value for controlling full charges, such as for electric vehicle applications. A future paper will disclose more advanced reduced-order methods to compute lithium plating for prolonged charge events as well as short charge events.

We make one final comment regarding efficiency. The speedup of the ROM versus PDE solutions can be much greater than the aforementioned 5000:1 if the ROM solutions are pre-computed and stored in a table and accessed via table lookup. Subsequently, "computing" any value of $\bar{j}_{s,\mathrm{ROM}}$ would be nearly instantaneous. We note that the ROM solution changes as the film resistance changes, but the film resistance changes very slowly. The entire table might be updated by the battery management system once per operational period (e.g., once per day), and then utilized throughout that operational period for significant performance gains.

5. Conclusions

From the results above, we see excellent correlation for the rate of lithium deposition on overcharge between a full-order coupled multi-physics PDE model and the reduced-order model derived in this paper. The reduced order model takes the very difficult and time consuming procedure to calculate the governing equations

necessary to obtain $\bar{j}_s$ in a PDE model, and reduces them to a very fast algebraic procedure that a small microcontroller can easily calculate. As noted, the speedup is at least 5000:1 when using the ROM versus the PDE solver, and can be made much faster via the proposed table-lookup approach to storing results.

Of particular importance, the reduced-order model is able to closely but conservatively predict the boundary between when lithium plating will not and will occur in the SOC/charge–current space, especially for short-duration charge events. This boundary is critical for producing controls that will not prematurely age a cell due to overcharge. In a future paper, the authors will explain their current research into optimal charging profiles that consider overcharge as well as other degradation mechanisms.

Improvements to the ROM might be possible if the assumptions made in Section 3 can be relaxed. In particular, Assumption 3 is not very accurate at high rates of charge. However, we find the present results to be adequate for initial development of control algorithms for battery charging.

List of symbols

a	specific surface area of porous electrode (m^{-1})
c	concentration of Li or Li^+ ions ($mol\,m^{-3}$)
D	diffusion coefficient ($m^2\,s^{-1}$)
E	composite quantity defined to ease notation per Eq. (19) ($V\,m^{-2}$)
F	Faraday's constant (96 487 $C\,mol^{-1}$)
i_e	current density of electrolyte ($A\,m^{-2}$)
i_0	exchange-current density for intercalation reaction ($A\,m^{-2}$)
i_{se}	current density of solid-electrolyte interface ($A\,m^{-2}$)
$i_{0,s}$	exchange-current density for side reaction ($A\,m^{-2}$)
j	local volumetric current density for intercalation reaction ($A\,m^{-3}$)
j_s	local volumetric current density for side reaction ($A\,m^{-3}$)
k	rate constant of electrochemical reaction ($A\,m^{5/2}\,mol^{-3/2}$)
L	length of cell or electrode (m)
P	composite quantity defined to ease notation per Eq. (23) (V)
Q	cell capacity (C)
R	particle radius (μm)
R_{film}	film resistance at the electrode/electrolyte interface ($\Omega\,m^2$)
R_g	universal gas constant ($8.314\,J\,mol^{-1}\,K^{-1}$)
T	temperature (K)
t	time (s)
t_0^+	transport number
U	local equilibrium potential (V)
x	length dimension (m)

Greek

α_a, α_c	anodic and cathodic transfer coefficients of electrochemical reaction
ε	volume fraction of a phase
ϕ	local potential of a phase (V)
η	local overpotential driving electrochemical reaction (V)
κ	conductivity of electrolyte ($S\,m^{-1}$)
θ	state-of-charge or stoichiometry of electrode
σ	conductivity of electrode ($S\,m^{-1}$)
ρ	density of active material ($kg\,m^{-3}$)
δ	film thickness (m)

Subscript/superscript

e	pertaining to the electrolyte phase
s	pertaining to the solid phase
n	pertaining to the negative electrode
p	pertaining to the positive electrode

Acknowledgments

Financial support for the research reported in this paper has been received from the General Motors/University of Michigan Advanced Battery Coalition for Drivetrains (GM/UM ABCD), to which the University of Colorado Colorado Springs is a subcontractor.

References

[1] M. Broussely, P. Biensan, F. Bonhomme, P. Blanchard, S. Herreyre, K. Nechev, R. Staniewicz, Journal of Power Sources 146 (2005) 90–96.
[2] M. Broussely, S. Herreyre, P. Biensan, P. Kasztejna, K. Nechev, R. Staniewicz, Journal of Power Sources 97–98 (2001) 13–21.
[3] R. Darling, J. Newman, Journal of the Electrochemical Society 145 (1998) 990–998.
[4] M. Doyle, T.F. Fuller, J. Newman, Journal of the Electrochemical Society 140 (1993) 1526–1533.
[5] T.F. Fuller, M. Doyle, J. Newman, Journal of the Electrochemical Society 141 (1994) 1–10.
[6] M.D. Levi, G. Salitra, B. Markovsky, H. Teller, D. Aurbach, U. Heider, L. Heider, Journal of the Electrochemical Society 146 (1999) 1279–1289.
[7] M.D. Levi, D. Aurbach, Journal of Electroanalytical Chemistry 421 (1997) 79–88.
[8] J. Vetter, P. Novák, M. Wagner, C. Veit, K.-C. Möller, J. Besenhard, M. Winter, M. Wohlfahrt-Mehrens, C. Vogler, A. Hammouche, Journal of Power Sources 147 (2005) 269–281.
[9] P. Arora, M. Doyle, R.E. White, Journal of the Electrochemical Society 146 (1999) 3543–3553.
[10] S. Moura, J. Forman, S. Bashash, J. Stein, H. Fathy, IEEE Transactions on Industrial Electronics 58 (2011) 3555–3566.
[11] N.A. Chaturvedi, R. Klein, J. Christensen, J. Ahmed, A. Kojic, IEEE Control Systems Magazine 30 (2010) 49–68.
[12] K.A. Smith, C.D. Rahn, C.-Y. Wang, Energy Conversion and Management 48 (2007) 2565–2578.
[13] COMSOL Multiphysics. http://www.comsol.com/ (accessed 24.10.11).
[14] MATLAB. http://www.mathworks.com/ (accessed 24.10.11).